

Tandem Native Mass-Spectrometry on Antibody–Drug Conjugates and Submillion Da Antibody–Antigen Protein Assemblies on an Orbitrap EMR Equipped with a High-Mass Quadrupole Mass Selector

Andrey Dyachenko,^{†,‡} Guanbo Wang,^{†,‡} Mike Belov,[§] Alexander Makarov,^{†,§} Rob N. de Jong,^{||} Ewald T. J. van den Bremer,^{||} Paul W. H. I. Parren,^{||,⊥} and Albert J. R. Heck^{*,†,‡}

[†]Biomolecular Mass Spectrometry and Proteomics, Bijvoet Centre for Biomolecular Research and Utrecht Institute for Pharmaceutical Sciences, University of Utrecht, Padualaan 8, 3584 CH, Utrecht, The Netherlands

[‡]Netherlands Proteomics Center, Padualaan 8, 3584 CH, Utrecht, The Netherlands

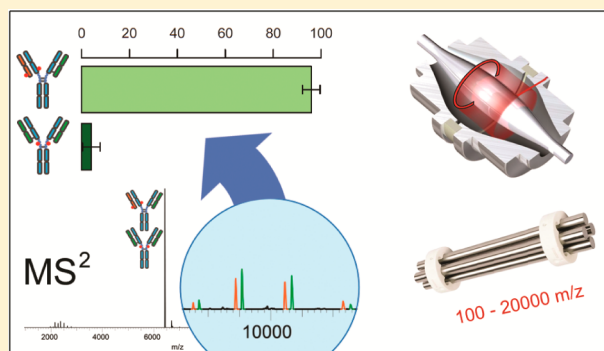
[§]Thermo Fisher Scientific, Bremen, Germany

^{||}Genmab, Utrecht, The Netherlands

[⊥]Department of Immunohematology and Blood Transfusion, Leiden University Medical Center, 2333 ZA Leiden, The Netherlands

Supporting Information

ABSTRACT: Native mass spectrometry is emerging as a powerful tool for the characterization of intact antibodies and antibody-based therapeutics. Here, we demonstrate new possibilities provided by the implementation of a high mass quadrupole mass selector on the recently introduced Orbitrap Exactive EMR mass spectrometer. This configuration allows precursor ion selection, and thus tandem mass spectrometry experiments, even on analytes with masses in the hundreds of kilodaltons. We apply tandem mass spectrometry to localize the drug molecules in the therapeutic antibody–drug conjugate brentuximab vedotin, which displays a heterogeneous drug load. Our tandem MS data reveal that drug conjugation takes place nonhomogeneously to cysteine residues both on the light and heavy chains. Next, we analyzed how many antigens bind to IgG hexamers, based on a recently described antibody mutant IgG1-RGY that forms hexamers and activates complement in solution. The fully saturated IgG1-RGY–antigen complexes displayed a stoichiometry of IgG:CD38 of 6:12, possessing a molecular weight of about 1.26 MDa and demonstrating that IgG assembly does not hamper antigen binding. Through tandem MS experiments, we retrieve information about the spatial arrangement and stoichiometry of the subunits within this complex. These examples underscore the potential of this further modified Orbitrap-EMR instrument especially for the in-depth characterization by native tandem mass spectrometry of antibodies and antibody-based constructs.



■ INTRODUCTION

Antibodies play an important role in modern pharmacology. New antibody-based targeted therapeutics against a wide range of diseases are rapidly emerging. Presently, several antibody–drug conjugates (ADC) are explored and have been approved for clinical use as they hold considerable promise in the treatment of various types of cancer. The ADC approach increases the therapeutic window of highly toxic small molecule drugs by combining it with the target specificity of monoclonal antibodies (mAbs). In addition, the pharmacokinetics of the ADC compare to that of the IgG1 antibody, resulting in a long in vivo half-life of the drug.^{1,2}

The majority of therapeutic ADCs are derived from the immunoglobulin G (IgG) class of antibodies. Structurally, IgG's are homo-heterodimers consisting of two “light” and two “heavy” polypeptide chains linked together by several disulfide bridges. IgG subunits may accommodate a variety of other post-

translational modifications (PTM) that affect their clearance, affinity, and specificity. The most common modification that is found on all the IgG molecules is the N-glycosylation of the heavy chain Asn297.

In ADCs, the drugs need to be conjugated to the IgG, which typically is done by coupling either via the naturally available lysine side chain amino groups or the cysteine thiol groups, formed upon partial reduction of IgG intermolecular disulfide bonds.³ More advanced strategies are being explored that use genetically pre-engineered cysteines,^{4,5} unnatural amino acids,⁶ or native glycans⁷ as a drug-conjugation site. Although these specific conjugation strategies allow for much better control over the drug load to the mAb, the ADCs that have currently

Received: February 16, 2015

Accepted: May 15, 2015

Published: May 15, 2015



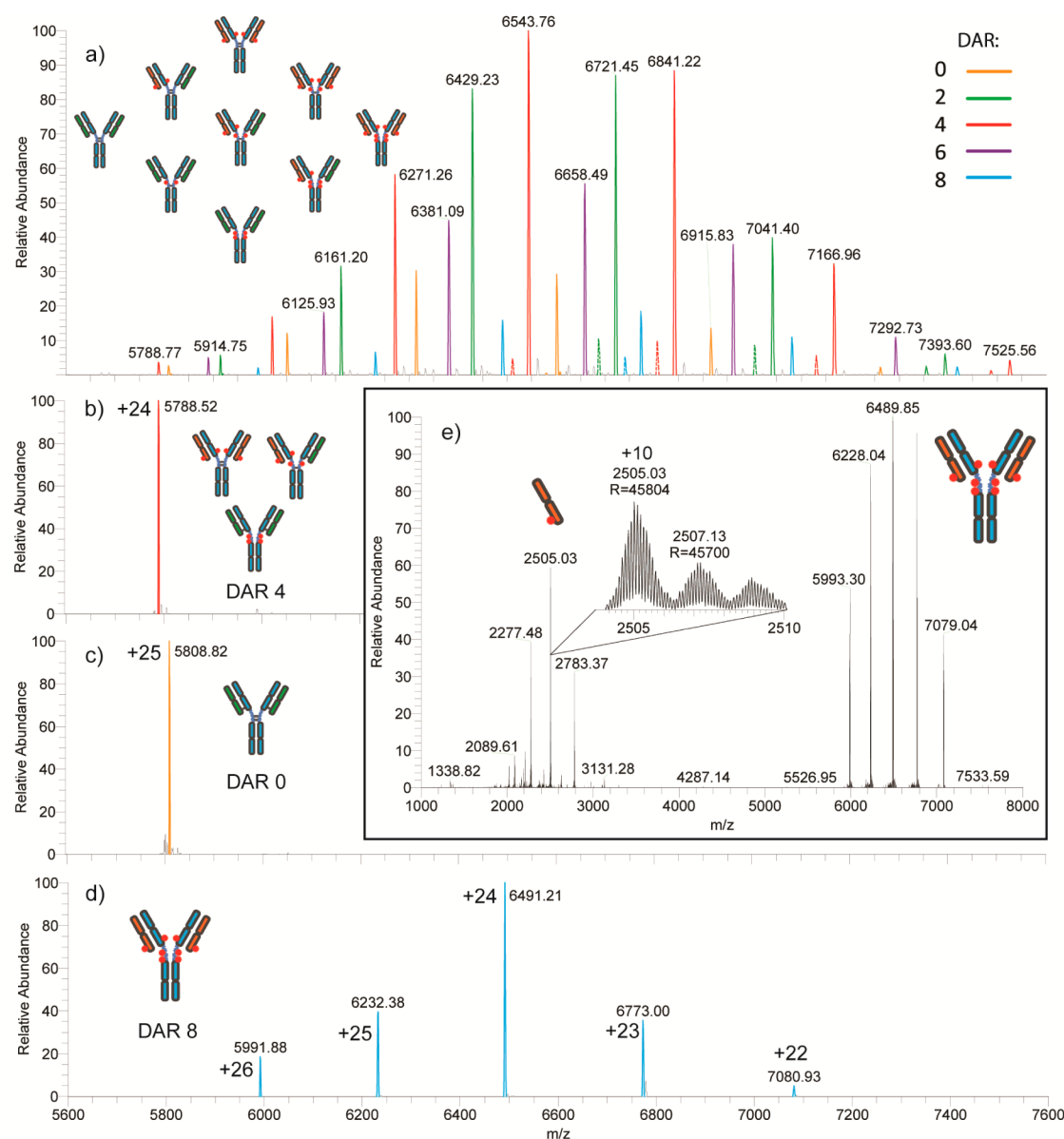


Figure 1. (a) Native ESI-MS high-resolution mass spectrum of the ADC Brentuximab vedotin. The charge state envelopes of each species with different DARs are color coded; the inset depicts a schematic of the nine potential positional isomers. (b,c) Selective precursor ion isolation by the high mass quadrupole of the DAR4 +24 charge state and DAR0 +25 charge state that are separated by 20 m/z units, respectively. The ion signal loss constituted about 9% for the DAR4 +24 peak and about 3% for the DAR0 +25 peak. (d) Selective DAR species isolation by spectrum multiplexing applied to isolation of all DAR8 ions present in the full MS spectrum. (e) Collision-induced dissociation of all DAR8 species selected by spectrum multiplexing acquired at a high resolution with 512 ms transient time allowing observation of the light chain fragment ions with isotopic resolution.

been approved for human use make use of lysine and cysteine residues naturally occurring in the IgG.² The resulting ADCs are often heterogeneous in terms of number of drug molecules bound per IgG and their distribution across the antibody, which presents a considerable challenge for current analytical techniques and calls for the development of new efficient characterization methods.^{8–12} Especially the ADCs created by coupling the drug-linker moieties to partially reduced interchain disulfide bridges present challenges as their quaternary intact structure in the absence of the disulfide bridges is preserved by noncovalent interactions. Therefore, it is highly desirable to perform the analysis under near-native conditions, as this potentially provides specific information about species with different drug-to-antibody ratios (DARs). One method for ADC separation that is compatible with physiological neutral

buffers is hydrophobic interaction chromatography (HIC).^{13,14} It exploits the increased hydrophobicity introduced to the antibody by conjugation with the drug linker, efficiently separating ADC with different DARs. However, the HIC-compatible buffers contain large amounts of nonvolatile salts, making them less suitable for direct coupling with a mass spectrometer.

Native mass spectrometry has gained substantial ground as a fast and efficient tool for the analysis of antibodies,^{15,16} antibody derivatives,^{17,18} and antibody–antigen complexes.^{19,20} In particular, we demonstrated that high resolution Orbitrap native mass spectrometry allows the extensive characterization of intact antibodies, including their glycosylation pattern, and also antibody drug conjugates.^{21–24} Until recently, native Orbitrap mass spectrometry of high m/z ions was limited to

the experiments on the entire ion population because commercial Orbitrap Exactive EMR instruments lacked the ability to isolate ions with m/z ratios over 4000. Belov et al. recently described a modified Orbitrap Exactive EMR mass spectrometer equipped with an ion funnel and a high mass quadrupole mass filter that was optimized for the transmission and isolation of the ions within the extended mass range.²⁵ On this instrument, they were able to achieve efficient isolation of native protein complex ions with molecular weights of over a few hundred kilodaltons.

Here, we also implemented a high mass quadrupole on an Orbitrap Exactive EMR mass spectrometer that had been previously modified for efficient transmission and detection of high molecular weight ions.^{26,27} The high mass quadrupole provides the ability to perform tandem mass spectrometry of native protein assemblies. We applied this new feature to assess the heterogeneity of brentuximab vedotin, a licensed ADC therapeutic, and demonstrate that the tandem mass spectrometry approach allows attainment of a level of characterization beyond just the DAR distribution, revealing information about drug localization across antibody molecules. Further, we analyzed very large antibody–antigen complexes, based on IgG hexamers, with molecular weights of around 1.26 MDa. Here, the high resolution provided by the mass analyzer turned out to be insufficient to determine the exact stoichiometry, primarily due to overlapping ion signals. By using tandem mass spectrometry, it was possible to monitor multiple consecutive dissociation events from the selected precursor ions, from which we derived that the main stoichiometry of the precursor ions was 6:12 for the IgG:antigen complex.

MATERIALS AND METHODS

More details on the materials, sample preparation procedures, and instrument modifications can be found in the Supporting Information.

Mass Spectrometry. All MS experiments were performed using an Orbitrap Exactive Plus mass spectrometer (Thermo Fisher Scientific, Bremen, Germany) modified for optimal transmission and detection of ions with m/z up to 50 000.^{27–29} For ion isolation, we used a standard quadrupole mass filter from a Q Exactive instrument with a modified electronic board that featured a decreased resonance frequency of 284 kHz and an upper mass-selection limit above 20000 m/z . Isolation windows of 5 Th and 3000 Th were used for tandem MS experiments with the ADCs and IgG:antigen complexes, respectively. The instrument, which is similar to that described by Belov et al., is depicted schematically as Supporting Information Figure S1.

RESULTS AND DISCUSSION

High-Resolution Tandem Mass Spectrometry of Brentuximab Vedotin. *Brentuximab Vedotin.* Brentuximab vedotin is an ADC licensed for the treatment of refractory Hodgkin lymphoma and systemic anaplastic large-cell lymphoma.³⁰ This ADC consists of a chimeric IgG1 antibody cAC10 conjugated to the cytotoxic payload, consisting of the tubulin inhibitor monomethyl auristatin E (MMAE) and a valine-citrulline cleavable linker.³¹ The linker is coupled to thiol groups of cysteine residues that are made available by partial reduction of interchain disulfide bridges in the IgG. There are four interchain disulfides in IgG1 that can potentially lead to drug conjugation. Two are in the flexible hinge region,

connecting the two IgG heavy chains, and two are in Fab region, pairing the light and heavy chains, resulting in a total of eight potential drug conjugation sites. Brentuximab vedotin is produced with an average DAR of around 4 because saturation of antibody with the drug molecules has a negative impact on the in vivo half-life and activity of the ADC.³² The resulting mixture contains species with a DAR of 0, 2, 4, 6, and 8 present as positional isomers³³ originating from the inhomogeneous drug distribution across the antibody (Figure 1a, inset).

Recently, we already demonstrated that, by using the Orbitrap Exactive EMR mass spectrometer adapted to the analysis of high molecular weight ions, it is possible to simultaneously assess the drug load and the glycosylation pattern of the ADC.²³ However, mere mass separation of the species with different drug loads does not fully resolve the heterogeneity of the cysteine-linked ADCs, as the drug localization sites can be distributed across eight different cysteine residues at the surface of the antibody. The location of the drug on the antibody can have a strong effect on its stability and pharmacokinetics;^{34,35} therefore, it is essential to be able to assess the distribution of the positional isomers in a quantitative manner. Recently, Le et al. successfully applied two orthogonal separation techniques (HIC + capillary electrophoresis (CE) and HIC + reversed phase HPLC) to establish the relative abundance of the positional isomers.³⁶ Here, we present an alternative complementary and more direct approach that utilizes native tandem mass spectrometry to assess the distribution of the drug localization sites in the ADC.

Ion Isolation Using the High Mass Quadrupole Mass Selector. The native MS spectrum of the intact deglycosylated brentuximab vedotin contains ion signals of five distinct species that correspond to the masses of the drug-free antibody and the ADC with DAR2, 4, 6, and 8 (Figure 1a, Table S1). The measured mass difference between the consecutive conjugation states is 2636.5 ± 1.5 Da, which agrees well with twice the theoretical mass of the drug-linker moiety vcMMAE (2637.3 Da). Isolation of individual peaks from such a crowded spectrum at m/z over 6000 can present a serious challenge for the mass filters that are currently commercially available. Here, we tested the performance of a high mass quadrupole mass filter incorporated in the modified Orbitrap Exactive Plus²⁸ instrument using it to isolate ion signals. To illustrate it, we chose two peaks with a relative abundance of less than 5% of the base peak that are separated in the spectrum by only 20 m/z : namely, the +24-charged DAR4 species carrying and the +25-charged DAR0 species (Figure 1b,c). Separating these peaks is challenging, as it requires high ion transmission through the narrow isolation window, dictated by the small distance between two peaks. The quadrupole isolation window is shaped close to a trapezoid with a longer side extending toward higher m/z .³⁷ In our experience, to achieve a clean isolation of two peaks at m/z around 6000, the isolation window has to be 2 to 4 times smaller than the distance to the closest peak. Here, we used the isolation window of 5 Th. As demonstrated by the clean isolation of the two peaks, we can achieve a resolution of over 300 at m/z of around 6000 without a noticeable loss of ion intensity, as illustrated by 91% and 97% transmission of DAR4 +24 and DAR0 +25 peaks, respectively (refer to SI for details on ion transmission calculation).

Ion isolation is usually the first step of a tandem MS experiment, followed by the ion activation and fragmentation. In cases where the intensity of a single ion species after isolation is insufficient, the resulting MSMS spectrum will be of

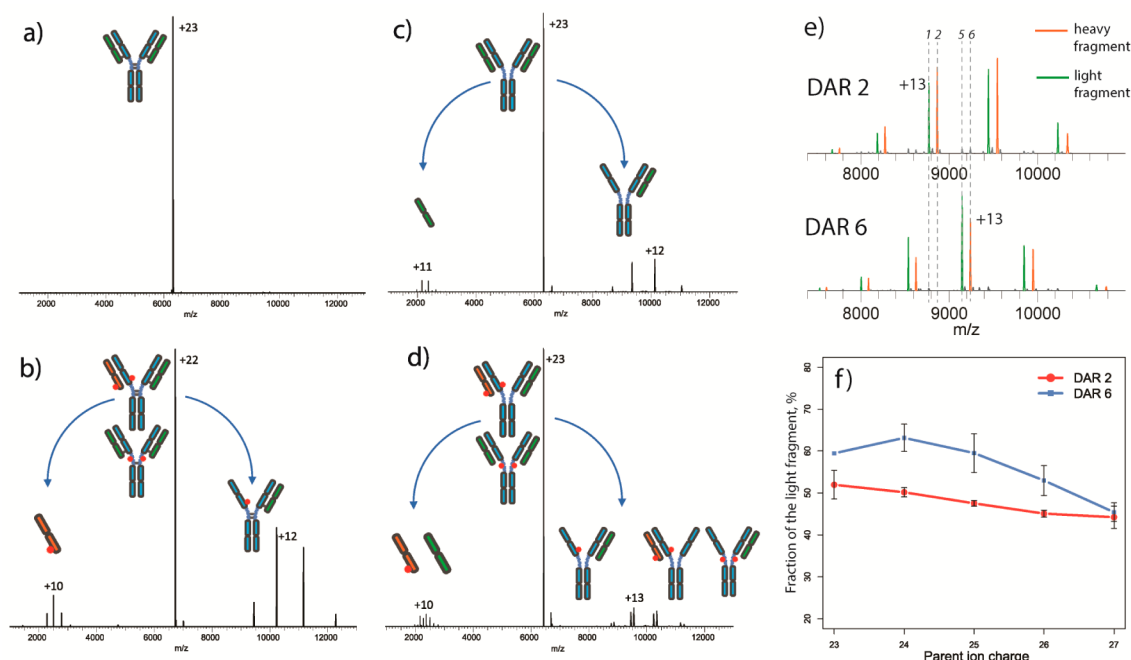


Figure 2. (a,b) Collision induced dissociation of selected nonreduced DAR0 and DAR2 precursor ions, respectively. DAR0 is resistant to fragmentation under these conditions, while DAR2 eliminates exclusively the drug-conjugated light chain. (c,d) Collision induced dissociation of the DTT reduced DAR0 and DAR2 species. Under these conditions, the DAR0 eliminates the light chain, and the DAR2 species eliminates both the drug-conjugated as well as the drug-free light chain. (e) Zoom-in on the fragment ions formed by the elimination of the light chain products from the reduced DAR2 and DAR6 species. Dashed lines with numbers indicate the number of drug molecules attached to a given fragment. (f) Percentage of the drug-conjugated light chain fragment in the total amount of the light-chain fragments plotted against parent ion charge state for DAR2 and DAR6 species.

poor quality and hard to interpret. This can be especially critical for the low-efficiency dissociation techniques like electron transfer dissociation (ETD)³⁸ or ultraviolet photodissociation (UVPD),³⁹ but also for large protein assemblies that often show remarkable resistance to dissociation. In such cases, it can be desirable to select multiple ions all belonging to the charge envelop of the same species, so that they can become activated and fragmented simultaneously. This can be achieved on the instrument described herein using a spectral multiplexing technique. The spectral multiplexing is implemented on the modified Exactive EMR system as follows: ions from a user-defined list are sequentially isolated by the quadrupole and sent to the HCD cell, fragmented there at an appropriate energy, and stored together with the previous products of precursors from the list. When the list is complete, all the products are transferred into the C-trap and analyzed in the Orbitrap simultaneously in a single spectrum. Using this method, it is possible to increase the signal-to-noise ratio of the fragments and improve the overall protein coverage. Demonstrating this utility we focused on the DAR8 species, representing the lowest abundant species in the native mass spectrum, comprising only about 7% of total ion intensity. We applied spectral multiplexing to isolate and simultaneously accumulate the charge states 22 to 26 of the DAR8 species (Figure 1d). In this case, the isolation window of 10 Th was sufficient to achieve a clean isolation of all five peaks and extract a complete low-abundant charge state envelope from a densely populated heterogeneous mass spectrum.

Tandem Mass Spectrometry of Native Brentuximab Vedotin. Under native MS conditions, the ADC containing partially reduced interchain disulfide bonds is kept intact primarily by the noncovalent interactions between subunits in

the CH3 and CH1 domains.⁴⁰ Ion isolation followed by gentle collisional activation can disrupt these noncovalent interactions, producing characteristic fragment ions. We used the high-mass quadrupole filter to isolate species with different DARs. If not stated otherwise, the isolation window of 5 Th and the acceleration voltage of 75 V were used for ion isolation and dissociation, respectively. First, we performed a collisional activation of the drug-free antibody (DAR0). At an activation energy of 75 eV, we did not observe any substantial fragmentation, indicating that under these circumstances DAR0 is resistant to dissociation (Figure 2a). Isolation and collisional activation of the DAR2 species under identical conditions lead to efficient dissociation, producing two fragment ions, namely the drug-conjugated light chain (LC_D) and concomitantly the ADC having lost the drug-conjugated LC_D (Figure 2b). Notably, no nondrug bound light chain was detected as a fragment ion. This fact together with the absence of fragmentation of the DAR0 species provides strong evidence that the selective disruption of the interchain disulfide bridges in brentuximab vedotin at the sites where the drug payload is attached destabilizes the LC:HC interaction. The disulfides that were not involved in the drug conjugation remain intact.

Interestingly, we detected no dissociation at the Fc–Fc interface even for the species with higher DARs, e.g. DAR8. This may be due to the fact that in CID of protein assemblies, typically the elimination of low mass fragments is the preferred pathway.⁴¹ Moreover in IgG1, the noncovalent Fc–Fc interaction is still strong, even when there are no disulfide bridges,⁴² which may prevent gas phase dissociation of the ADC.⁴⁰ To study fine details of fragment ions, it may be important to examine them with very accurate masses and thus at isotopic resolution. With a molecular weight of 25 kDa, the

drug-conjugated light chain fragment ions require a resolution better than 25 000 to reveal their isotopic fine structure and thus long transient times on the Orbitrap. As the ion signal in the Orbitrap decays significantly over such transient times, we needed to compensate the loss of the signal by performing the above-described spectral multiplexing for precursor species isolation. We applied spectral multiplexing followed by collisional activation at 75 eV to the low-abundant DAR8 species (Figure 1e). After isolating five charge states of DAR8, we attained enough signal to reach a resolution of over 45 000 at m/z of 2500 and resolve the isotopic structure of the drug-conjugated light chain.

Tandem MS of Native Reduced Brentuximab Vedotin. In native tandem MS, all the drug-conjugated ADCs followed the same dissociation pathway, by exclusively eliminating the drug-conjugated light chain. This is an indication that the reduction of a disulfide bond is required for the dissociation of the light chain. With this in mind, we treated the ADC with dithiothreitol (DTT) in order to reduce interchain disulfides enabling the dissociation of the free light chain. The integrity of the partially reduced albeit still intact ADC was confirmed by native mass spectrometry (Figure S2). We next examined the dissociation pathways of the reduced ADC by isolating the individual conjugated species with the high-mass quadrupole and exposing them to collisional activation in the HCD cell.

As expected, the reduced ADCs dissociate, producing fragment ions that are distinct from the untreated ADC. Now the reduced DAR0 species does dissociate via the elimination of the light chain that is clearly made possible by the disulfide bond reduction (Figure 2c). The drug-conjugated ADCs do now eliminate both drug-conjugated as well as drug-free light chains. As illustrated in Figure 1a, the species DAR2, DAR4, and DAR6 each may be comprised of a mixture of different positional isomers. Having the same mass, these isomers are indistinguishable at the intact protein level. Similarly, collisional dissociation of the ADC in the nonreduced form does not provide quantitative information about the drug localization due to the presence of only one dissociation pathway. On the contrary, the partially reduced ADC, when subjected to high energy collisions with inert gas, dissociates through two distinct pathways. Namely, either the free light chain or drug-conjugated light chain is eliminated, resulting in formation of two populations of fragments. In the case of DAR2, the corresponding “heavy” and “light” fragments contain 2 or 1 conjugated drugs, respectively. They are mass separated by 1318.6 Da and therefore can be distinguished by mass spectrometry (Figure 2d,e) and semiquantified. Similarly, dissociation of the DAR6 species results in two types of the high mass fragments that correspond to five and six conjugated drug molecules (Figure 2e).

We further investigated fragmentation efficiencies of the free vs drug-conjugated light chain by fragmenting +23 charge states of DAR0 and DAR2 species under the same experimental conditions (Figure S3). The ratios between the intensity of the precursor and collective intensity of fragment ions were 79.8:20.2 and 79.1:20.9 for DAR0 and DAR2, respectively, suggesting similar dissociation efficiencies of free and drug-conjugated light chain.

Next, we performed tandem MS experiments on the individual charge states 23 to 27 of reduced forms of DAR2 and DAR6 and calculated the percentage of the drug-conjugated light chain compared to the total amount of light chain fragments (Figure 2f) to estimate the stoichiometry of the

drug load specific to the light chains. The subtle although significant charge-state dependence of the percentage of the drug-conjugated light chain indicates that different positional isomers may have different protonation characteristics in the electrospray ionization. Still, from these data, we can extract information on the distribution of the drug molecules over the available sites in the ADC.

Relative Abundance of Positional Isomers in DAR2 and DAR6. As species with odd DAR values are not present in the drug product, the number of possible positional isomers for the DAR2, DAR4, and DAR6 species is 3, 4, and 3, respectively, taking into account the 2-fold symmetry of the IgG1 molecule. Having just two experimental values given by the relative intensities of the fragment ions is not sufficient to quantify all isomers unambiguously. To reduce complexity, we separated the conjugation sites into two groups—the “Fab group” and the “hinge group”—and treated the sites within one group as equivalent, thus reducing the number of isomers. In the strict sense, this assumption is not valid for the hinge region disulfides, as they connect different amino acid residues. However, it has been shown that these two hinge disulfides express similar rates of reduction,⁴³ so treating them as equivalent is appropriate.

Theoretically, collisional activation of the DAR2 species with fully reduced interchain disulfide bridges and drugs conjugated to the hinge cysteines (DAR2_H) will exclusively proceed via the elimination of the free light chain. On the other hand, the reduced DAR2 with drug molecules on one of the Fab arms (DAR2_F) should fragment producing free or drug-conjugated light chain fragments with equal probability (Figure 2d). Therefore, the fractions of DAR2_F and DAR2_H can be expressed as $2I_{2L}$ and $1 - 2I_{2L}$ respectively, where I_{2L} is the relative abundance of the light fragment conjugated to one drug (Figure 2e). Similarly, the fractions of the DAR6 positional isomers (DAR6_{HHF} and DAR6_{HFF}) are equal to $2I_{6H}$ and $1 - 2I_{6H}$, where I_{6H} is a relative abundance of the heavy fragment conjugated to six drugs (Figure 2e). By combining these values with the drug load distribution obtained from the all-ion spectrum, it is possible to calculate the percentages of each positional isomer in the sample. The results are summarized in Table S2. We compared our calculated values with the recent results obtained by Le et al. on the similar ADC, albeit with somewhat lower drug load, whereby they used a combined HIC/CE-SDS approach.³⁶ We found a good agreement in relative distributions of the drug conjugation sites on DAR2 and DAR6. The overall percentages of the positional isomers do not exactly match, likely due to the smaller average drug conjugation load of the ADC used by Le et al. This example highlights the added value of high-resolution native tandem mass spectrometry as a tool for the characterization of cysteine-linked ADCs.

High-Resolution Tandem Mass Spectrometry of Macromolecular Antibody–Antigen Assemblies. The IgG1-RGY Mutant Assembles into Hexamers Spontaneously.

Antibodies play a vital role in adaptive immunity. Recently, we elucidated the mechanism by which IgG antibodies mediate complementary activation at the molecular level, which was shown to occur through the formation of ordered hexameric IgG assemblies following antigen binding on the cell surface. These complexes bind to the C1 subunit, which is the initial step in complement activation, leading to the generation of opsonins, chemoattractants, and membrane attack complexes.⁴⁴ We demonstrated that the propensity to hexamerize at the cell

surface can be enhanced via the introduction of certain Fc:Fc interface mutations, which can thus possibly lead to a new class of hexameric therapeutic antibodies with stronger complement activating capability. We demonstrated that an IgG1 triple mutant, IgG1-RGY, showed increased hexamerization compared to single mutants, in which IgG1-RGY hexamers were also detectable in solution.⁴⁴ The IgG1-RGY mutant therefore provides an excellent model system for studying the spatial organization of the IgG's in the hexameric assemblies. The model of IgG1 hexamers bound to the cell surface as developed in Diebold et al.⁴⁴ suggests that IgG1 molecules solely interacted through the Fc regions, in which a single Fab arm of each antibody bound surface-bound antigen (i.e., one Fab arm but not two Fab arms simultaneously engaging antigen in the IgG1 hexamer-C1 complex). This poses the question whether hexamer formation as such prohibits bivalent antibody binding to the antigen. Here, we use high-resolution native tandem mass-spectrometry to elucidate the molecular interactions of a solution-phase IgG1-RGY CD38 antibody hexamer in complex with soluble CD38 antigen (sCD38).

High-Resolution Native MS of Hexameric IgG1:sCD38 Protein Assemblies. We examined the interactions of sCD38 with the anti-CD38 antibody triple mutant (IgG1-005-RGY, $K_D = 6$ nM).⁴⁵ As a negative control, we used the anti-EGFR antibody (IgG1-2F8-RGY) that does not interact with CD38. The IgG1-RGY antibodies were incubated with sCD38 for 30 min at an sCD38:IgG1 mixing ratio of 2.5 and the complexes formed were analyzed using the modified Exactive EMR instrument. The IgG1 hexamer (IgG1₆) is a fairly large 890 kDa noncovalent assembly. Therefore, the mass-spectrometric analysis of IgG1₆ is challenging as it requires a combination of higher accelerating voltages on the ions optics for efficient ion transmission and desolvation, but we also need to restrict collisional activation to preserve the intact protein assemblies. We replaced the nitrogen in the HCD cell of our modified Exactive Plus with the heavier xenon to enhance collisional cooling.²⁷ Still, careful manual tuning of the transmission optics DC voltages was required to obtain stable and abundant ion signals.

For both IgG1-005-RGY and IgG1-2F8-RGY, we predominantly detected monomers (IgG1₁) and hexamers (IgG1₆), although to a lesser extent we also observed IgG1₂, IgG1₃, and IgG1₄ species (Figure 3a,b). In our negative control, indeed no IgG1-2F8-RGY:sCD38 complexes were detected (Figure 3a, Table S3). In contrast, the IgG1-005-RGY readily formed a specific complex with sCD38, which is reflected by the significant mass shifts in the native ESI-MS spectrum (Figure 3b). In this spectrum, the peaks corresponding to monomeric IgG1 can be unambiguously assigned to a 1:2 IgG1-RGY:sCD38 complex (Table S4). However, the assignment of the peak envelope that corresponds to the complex of IgG1₆ with sCD38 is not unambiguous. Considerable peak broadening suggests that they may correspond to several partially overlapping species. To further investigate this, we simulated spectra of IgG1₆:sCD38₁₀, IgG1₆:sCD38₁₁, IgG1₆:sCD38₁₂, and IgG1₆:sCD38₁₃ (Figure 3c, inset). We superimposed the simulated spectra over the experimental one and demonstrated that in this m/z region, different binding stoichiometries overlap partially, hampering peak assignments.

Tandem MS of Hexameric IgG1-RGY:sCD38 Protein Assemblies Enables Determination of the Stoichiometry. We argued that this ambiguity could be resolved by tandem mass spectrometry.^{27,46} Unfortunately, isolation and collisional

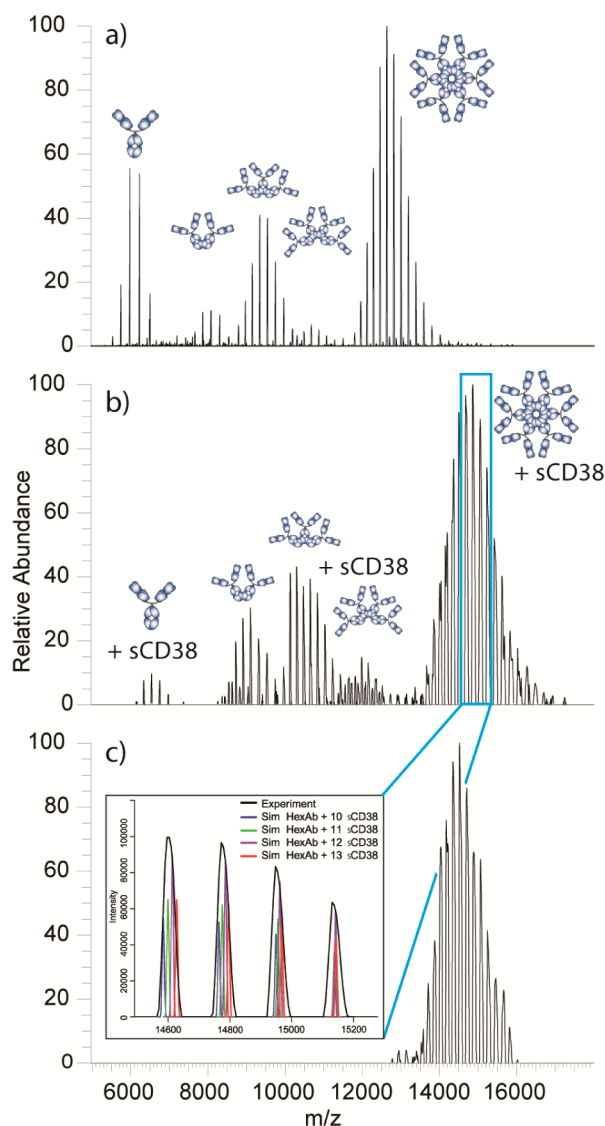


Figure 3. (a) Native ESI-MS high-resolution mass spectrum of the hexameric IgG1-2F8 antibody with 2.5 equiv (monomer:monomer ratio) of the nonrecognized nonglycosylated antigen CD38. (b) Native ESI-MS high-resolution mass spectrum of the hexameric IgG1-005 antibody targeting CD38 with 2.5 equiv of nonglycosylated CD38. (c) Broadband precursor ion isolation of the antibody hexamer in complex with CD38 antigen molecules. The inset shows the simulated spectra of IgG1-005 hexamer:CD38 complex at different IgG's to CD38 stoichiometries.

dissociation of a single IgG1₆:sCD38_x peak did not provide a sufficient signal under CID conditions, likely caused by substantial signal loss when isolating and manipulating high mass ions. To gain more signal, we applied broadband isolation with a 3000 m/z isolation window to separate and selectively activate the entire IgG1₆:sCD38_x peak envelope (Figure 3c), thereby eliminating lower order IgG assemblies. By increasing the HCD acceleration voltage from 100 to 200 V, we were able to follow the dissociation of the IgG1₆:sCD38_x assemblies step-by-step (Figure 4a,b,c).

It is generally observed that the order of gas-phase subunit dissociation can be correlated with the spatial arrangement of the subunits in the complex, whereby looser attached peripheral subunits are lost more facily.^{47–49} For the IgG1₆:sCD38_x

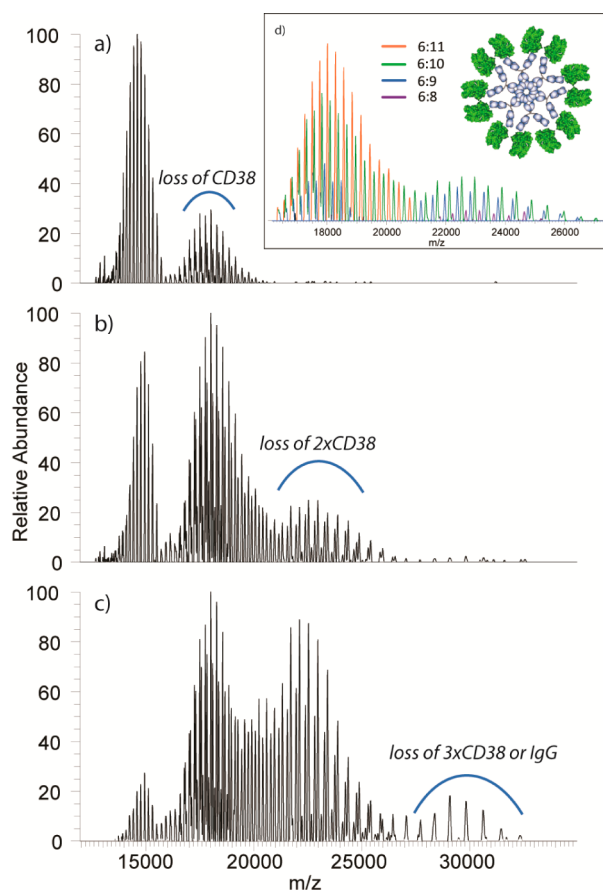


Figure 4. Broadband isolation of the antibody hexamer in complex with CD38 antigen molecules followed by collisional dissociation at acceleration voltages of (a) 100 V, (b) 150 V, and (c) 200 V. (d) Color annotation of fragment ions produced by collisional dissociation of the IgG1–005 hexamer:CD38 complex at 150 V colored according to the number of CD38 subunits present; the inset schematically shows suggested spatial arrangement of the subunits in the complex. As the dominated fragment ions series corresponds to an IgG:CD38 complex of 6:11, the dominant precursor ions should have been the 6:12 IgG:CD38 complex.

complex, the increase of acceleration voltage in the HCD cell up to 150 V resulted in the elimination of two consecutive sCD38 antigens (Figure 4a, b). A further increase of the acceleration voltage up to the current hardware limit of 200 V results in the release of a third sCD38 with the additional minor dissociation pathway comprising the loss of one core IgG1 subunit, as confirmed by the simulation (Figure 4c, Figure S4). To determine the stoichiometry of the IgG₁:sCD38_x precursor assemblies, we analyzed the fragmentation pattern at 150 V acceleration voltage. Charge partition upon CID allowed better peak separation and made it possible to unambiguously assign all the ion series present in the tandem MS spectrum (Figure 4d). After dissociation of the first sCD38 subunit, the most abundant species observed was IgG₁:sCD38₁₁, followed by IgG₁:sCD38₁₀ and IgG₁:sCD38₉. Likewise, the second CD38 dissociation produced IgG₁:sCD38₁₀, followed by IgG₁:sCD38₉ and IgG₁:sCD38₈ (Table S5). This suggests that the precursor ion assembly is present in three different stoichiometries: IgG₁:sCD38₁₂, IgG₁:sCD38₁₁, and IgG₁:sCD38₁₀. Notably, no IgG₁:sCD38₁₃ is present as a precursor, already indicating the hexameric IgG's bind up to 12 antigens at above saturated

antigen concentrations. The relative abundance of the precursor ions IgG₁:sCD38₁₂, IgG₁:sCD38₁₁, and IgG₁:sCD38₁₀ can be estimated from the relative abundances of the corresponding fragment ions to be 0.52:0.38:0.10, respectively (Table S6). The relative abundances in the corresponding monomeric wild type IgG1–005 with sCD38 are about 0.95:0.05 (Figure S5). When IgG1 hexamerization would have no effect on antibody–antigen affinity, we would expect relative abundances of IgG₁:sCD38₁₂, IgG₁:sCD38₁₁, and IgG₁:sCD38₁₀ of 0.74:0.23:0.03. This may indicate that the interactions between the CD38 antigen and the Fab arms of the IgG1–005-RGY antibody are just slightly more constrained in the case of IgG hexamer as compared to a monomeric IgG1. However, the differences are rather marginal and can also originate from sample handling. We conclude therefore that IgG hexamerization does not preclude bivalent antigen binding.

CONCLUSIONS

Here, we report on the implementation of a high-mass quadrupole mass filter on our previously described modified Orbitrap Exactive Plus mass spectrometer,^{28,29} optimized for efficient transmission and detection of the high-mass biomolecular ions. We demonstrate how this implementation allows us to analyze antibody based products by tandem mass spectrometry. Using this new workflow, not only can we probe the heterogeneity in stoichiometry of the drug conjugation in ADCs but we can also retrieve data on the site-specific location of the drugs in the antibodies. Moreover, tandem mass spectrometry allowed us to unambiguously probe the stoichiometry of antigen binding, even in IgG₆-antigen protein assemblies with molecular weights over 1 million Da. We expect that this work expands the repertoire of analytical techniques available for the characterization of antibodies and antibody-based constructs, contributing analytical tools needed for the development of more potent therapeutics.

ASSOCIATED CONTENT

Supporting Information

Materials and methods, supporting figures, and supporting tables. The Supporting Information is available free of charge on the ACS Publications website at DOI: 10.1021/acs.analchem.5b00788.

AUTHOR INFORMATION

Corresponding Author

*E-mail: a.j.r.heck@uu.nl.

Notes

The authors declare the following competing financial interest(s): M. Belov and A. Makarov are employees of ThermoFisher Scientific, who commercialize the described Orbitrap EMR. R. N. de Jong, E. T. J. van den Bremer, and P. W. H. I. Parren are employees of Genmab, who developed, produce, and commercialize the hexameric IgG platforms described here.

ACKNOWLEDGMENTS

We thank all (former) members of the Heck lab for help, especially Sara Rosati, Joost Snijder, and Arjen Barendregt. This research was performed within the framework of The Netherlands Organization for Scientific Research (NWO) and supported by the large scale proteomics facility *Proteins@Work*

(project 184.032.201) embedded in The Netherlands Proteomics Centre.

REFERENCES

- (1) Beck, A.; Reichert, J. M. *mAbs* **2013**, *6*, 15–17.
- (2) Chari, R. V. J.; Miller, M. L.; Widdison, W. C. *Angew. Chem., Int. Ed. Engl.* **2014**, *53*, 3796–3827.
- (3) Beck, A.; Haeuw, J.-F.; Wurch, T.; Goetsch, L.; Bailly, C.; Corvaia, N. *Discovery Med.* **2010**, *10*, 329–339.
- (4) Junutula, J. R.; Raab, H.; Clark, S.; Bhakta, S.; Leipold, D. D.; Weir, S.; Chen, Y.; Simpson, M.; Tsai, S. P.; Dennis, M. S.; Lu, Y.; Meng, Y. G.; Ng, C.; Yang, J.; Lee, C. C.; Duenas, E.; Gorrell, J.; Katta, V.; Kim, A.; McDorman, K.; Flagella, K.; Venook, R.; Ross, S.; Spencer, S. D.; Lee Wong, W.; Lowman, H. B.; Vandlen, R.; Sliwkowski, M. X.; Scheller, R. H.; Polakis, P.; Mallet, W. *Nat. Biotechnol.* **2008**, *26*, 925–932.
- (5) Bhakta, S.; Raab, H.; Junutula, J. R. *Methods Mol. Biol.* **2013**, *1045*, 189–203.
- (6) Axup, J. Y.; Bajjuri, K. M.; Ritland, M.; Hutchins, B. M.; Kim, C. H.; Kazane, S. A.; Halder, R.; Forsyth, J. S.; Santidrian, A. F.; Stafin, K.; Lu, Y.; Tran, H.; Sella, A. J.; Biroc, S. L.; Szydlak, A.; Pinkstaff, J. K.; Tian, F.; Sinha, S. C.; Felding-Habermann, B.; Smider, V. V.; Schultz, P. G. *Proc. Natl. Acad. Sci. U. S. A.* **2012**, *109*, 16101–16106.
- (7) Zhou, Q.; Stefano, J. E.; Manning, C.; Kyazike, J.; Chen, B.; Gianolio, D. A.; Park, A.; Busch, M.; Bird, J.; Zheng, X.; Simonds-Mannes, H.; Kim, J.; Gregory, R. C.; Miller, R. J.; Brondyk, W. H.; Dhal, P. K.; Pan, C. Q. *Bioconjugate Chem.* **2014**, *25*, 510–520.
- (8) Wakankar, A.; Chen, Y.; Gokarn, Y.; Jacobson, F. S. *mAbs* **2011**, *3*, 161–172.
- (9) Alley, S. C.; Anderson, K. E. *Curr. Opin. Chem. Biol.* **2013**, *17*, 406–411.
- (10) Gautier, V.; Boumeester, A. J.; Lössl, P. *Proteomics* **2015**, in press.
- (11) Valliere-Douglass, J. F.; Hengel, S. M.; Pan, L. Y. *Mol. Pharm.* **2014**, DOI: 10.1021/mp500614p.
- (12) Pan, L. Y.; Salas-Solano, O.; Valliere-Douglass, J. F. *Anal. Chem.* **2014**, *86*, 2657–2664.
- (13) Queiroz, J. A.; Tomaz, C. T.; Cabral, J. M. S. *J. Biotechnol.* **2001**, *87*, 143–159.
- (14) Haverick, M.; Mengisen, S.; Shameem, M.; Ambrogelly, A. *mAbs* **2014**, *6*, 852–858.
- (15) Thompson, N. J.; Rosati, S.; Heck, A. J. R. *Methods* **2013**, *1*–7.
- (16) Thompson, N. J.; Hendriks, L. J. a; de Kruif, J.; Throsby, M.; Heck, A. J. R. *mAbs* **2014**, *6*, 197–203.
- (17) Valliere-Douglass, J. F.; McFee, W. A.; Salas-Solano, O. *Anal. Chem.* **2012**, *84*, 2843–2849.
- (18) Hengel, S. M.; Sanderson, R.; Valliere-Douglass, J.; Nicholas, N.; Leiske, C.; Alley, S. C. *Anal. Chem.* **2014**, *86*, 3420–3425.
- (19) Atmanene, C.; Wagner-Rousset, E.; Malissard, M.; Chol, B.; Robert, A.; Corvaia, N.; Van Dorsselaer, A.; Beck, A.; Sanglier-Cianfèrani, S. *Anal. Chem.* **2009**, *81*, 6364–6373.
- (20) Debaene, F.; Wagner-Rousset, E.; Colas, O.; Ayoub, D.; Corvaia, N.; Van Dorsselaer, A.; Beck, A.; Cianfèrani, S. *Anal. Chem.* **2013**, *85*, 9785–9792.
- (21) Rosati, S.; Yang, Y.; Barendregt, A.; Heck, A. J. R. *Nat. Protoc.* **2014**, *9*, 967–976.
- (22) Debaene, F.; Boeuf, A.; Wagner-Rousset, E.; Colas, O.; Ayoub, D.; Corvaia, N.; Van Dorsselaer, A.; Beck, A.; Cianfèrani, S. *Anal. Chem.* **2014**, *86*, 10674.
- (23) Rosati, S.; van den Bremer, E. T.; Schuurman, J.; Parren, P. W.; Kamerling, J. P.; Heck, A. J. *mAbs* **2013**, *5*, 917–924.
- (24) Marcoux, J.; Champion, T.; Colas, O.; Wagner-Rousset, E.; Corvaia, N.; Van Dorsselaer, A.; Beck, A.; Cianfèrani, S. *Protein Sci.* **2015**, *00*, n/a–n/a.
- (25) Belov, M. E.; Damoc, E.; Denisov, E.; Compton, P. D.; Horning, S.; Makarov, A. a; Kelleher, N. L. *Anal. Chem.* **2013**, *85*, 11163–11173.
- (26) Rose, R. J.; Damoc, E.; Denisov, E.; Makarov, A.; Heck, A. J. R. *Nat. Methods* **2012**, *9*, 1084–1086.
- (27) Snijder, J.; van de Waterbeemd, M.; Damoc, E.; Denisov, E.; Grinfeld, D.; Bennett, A.; Agbandje-McKenna, M.; Makarov, A.; Heck, A. J. R. *J. Am. Chem. Soc.* **2014**, *136*, 7295–7299.
- (28) Rose, R.; Damoc, E.; Denisov, E.; Makarov, A.; Heck, A. *Nat. Methods* **2012**, *9*, 2–6.
- (29) Rosati, S.; Rose, R. J.; Thompson, N. J.; van Duijn, E.; Damoc, E.; Denisov, E.; Makarov, A.; Heck, A. J. R. *Angew. Chem., Int. Ed. Engl.* **2012**, *51*, 12992–12996.
- (30) Deng, C.; Pan, B.; O'Connor, O. a. *Clin. Cancer Res.* **2013**, *19*, 22–27.
- (31) Katz, J.; Janik, J. E.; Younes, A. *Clin. Cancer Res.* **2011**, *17*, 6428–6436.
- (32) Hamblett, K.; Senter, P.; Chace, D. *Clin. Cancer Res.* **2004**, *7063*–7070.
- (33) Janin-Bussat, M.-C.; Dillenbourg, M.; Corvaia, N.; Beck, A.; Klinguer-Hamour, C. *J. Chromatogr. B* **2015**, *981*–982, 9–13.
- (34) Strop, P.; Liu, S.-H.; Dorywalska, M.; Delaria, K.; Dushin, R. G.; Tran, T.-T.; Ho, W.-H.; Farias, S.; Casas, M. G.; Abdiche, Y.; Zhou, D.; Chandrasekaran, R.; Samain, C.; Loo, C.; Rossi, A.; Rickert, M.; Krimm, S.; Wong, T.; Chin, S. M.; Yu, J.; Dilley, J.; Chaparro-Riggers, J.; Filzen, G. F.; O'Donnell, C. J.; Wang, F.; Myers, J. S.; Pons, J.; Shelton, D. L.; Rajpal, A. *Chem. Biol.* **2013**, *20*, 161–167.
- (35) Shen, B.-Q.; Xu, K.; Liu, L.; Raab, H.; Bhakta, S.; Kenrick, M.; Parsons-Reponte, K. L.; Tien, J.; Yu, S.-F.; Mai, E.; Li, D.; Tibbitts, J.; Baudys, J.; Saad, O. M.; Scales, S. J.; McDonald, P. J.; Hass, P. E.; Eigenbrot, C.; Nguyen, T.; Solis, W. A.; Fujii, R. N.; Flagella, K. M.; Patel, D.; Spencer, S. D.; Khawli, L. A.; Ebens, A.; Wong, W. L.; Vandlen, R.; Kaur, S.; Sliwkowski, M. X.; Scheller, R. H.; Polakis, P.; Junutula, J. R. *Nat. Biotechnol.* **2012**, *30*, 184–189.
- (36) Le, L. N.; Moore, J. M. R.; Ouyang, J.; Chen, X.; Nguyen, M. D. H.; Galush, W. J. *Anal. Chem.* **2012**, *84*, 7479–7486.
- (37) Miller, P. E.; Denton, M. B. *J. Chem. Educ.* **1986**, *63*, 617.
- (38) Syka, J. E. P.; Coon, J. J.; Schroeder, M. J.; Shabanowitz, J.; Hunt, D. F. *Proc. Natl. Acad. Sci. U. S. A.* **2004**, *101*, 9528–9533.
- (39) Shaw, J. B.; Li, W.; Holden, D. D.; Zhang, Y.; Griep-Raming, J.; Fellers, R. T.; Early, B. P.; Thomas, P. M.; Kelleher, N. L.; Brodbelt, J. S. *J. Am. Chem. Soc.* **2013**, *135*, 12646–12651.
- (40) Rose, R. J.; Labrijn, A. F.; van den Bremer, E. T. J.; Loverix, S.; Lasters, I.; van Berkel, P. H. C.; van de Winkel, J. G. J.; Schuurman, J.; Parren, P. W. H. I.; Heck, A. J. R. *Structure* **2011**, *19*, 1274–1282.
- (41) Heck, A. J. R.; Van Den Heuvel, R. H. H. *Mass Spectrom. Rev.* **2004**, *23*, 368–389.
- (42) Rispens, T.; Davies, A. M.; Ooijevaar-de Heer, P.; Absalah, S.; Bende, O.; Sutton, B. J.; Vidarsson, G.; Aalberse, R. C. *J. Biol. Chem.* **2014**, *289*, 6098–6109.
- (43) Liu, H.; Chumsae, C.; Gaza-Bulsecu, G.; Hurkmans, K.; Radziejewski, C. H. *Anal. Chem.* **2010**, *82*, 5219–5226.
- (44) Diebold, C. a; Beurskens, F. J.; de Jong, R. N.; Koning, R. I.; Strumane, K.; Lindorfer, M. a; Voorhorst, M.; Ugurlar, D.; Rosati, S.; Heck, A. J. R.; van de Winkel, J. G. J.; Wilson, I. a; Koster, A. J.; Taylor, R. P.; Saphire, E. O.; Burton, D. R.; Schuurman, J.; Gros, P.; Parren, P. W. H. I. *Science* **2014**, *343*, 1260–1263.
- (45) De Weers, M.; Tai, Y.-T.; van der Veer, M. S.; Bakker, J. M.; Vink, T.; Jacobs, D. C. H.; Oomen, L. a; Peipp, M.; Valerius, T.; Sloodstra, J. W.; Mutis, T.; Bleeker, W. K.; Anderson, K. C.; Lokhorst, H. M.; van de Winkel, J. G. J.; Parren, P. W. H. I. *J. Immunol.* **2011**, *186*, 1840–1848.
- (46) Snijder, J.; Utrecht, C.; Rose, R. J.; Sanchez-Eugenio, R.; Marti, G. A.; Agirre, J.; Guérin, D. M. A.; Wuite, G. J. L.; Heck, A. J. R.; Roos, W. H. *Nat. Chem.* **2013**, *5*, 502–509.
- (47) Snijder, J.; Heck, A. J. R. *Annu. Rev. Anal. Chem. (Palo Alto, Calif)* **2014**, *7*, 43–64.
- (48) Lorenzen, K.; Vannini, A.; Cramer, P.; Heck, A. J. R. *Structure* **2007**, *15*, 1237–1245.
- (49) Wortham, N. C.; Martinez, M.; Gordiyenko, Y.; Robinson, C. V.; Proud, C. G. *FASEB J.* **2014**, *28*, 2225–2237.